Arab J. Nucl. Sci. Appl., Vol. 55, 2, 79-93 (2022)

ISSN 1110-0451

Arab Journal of Nuclear Sciences and Applications

Web site: ajnsa.journals.ekb.eg

(E S N S A)

Validation of k_0-Standardization Procedure of Instrumental Neutron Activation Analysis at Ghana Research Reactor-1 Facility for the Determination of Rare Earth Elements

Ebenezer Aquisman Asare [1,2*], Charles Kofi Klutse [2,5], Francis Yaw Acquaye [3,4]

[1] *Department of Chemistry, Faculty of Resource Science and Technology, Universiti Malaysia Sarawak, Malaysia*

[2] *Department of Nuclear Science and Applications, Graduate School of Nuclear and Allied Sciences, University of Ghana, AE1, Atomic – Accra, Ghana.*

[3] *Department of Chemistry and Biochemistry, College of Arts and Sciences, University of Alabama, Alabama, U.S.A.*

[4] *Department of Nuclear Engineering, Graduate School of Nuclear and Allied Sciences, University of Ghana, AE1, Atomic – Accra, Ghana.*

[5] *Nuclear Power Institute, Ghana Atomic Energy Commission, P. O. Box LG80, Legon – Accra, Ghana*

ARTICLE INFO

Article history:

Received: 16th Aug. 2021

Accepted: 29th Dec. 2021

Keywords:

Rare earth element;

Environmental reference material;

k_0-standardization technique;

Gamma-ray spectrometer.

ABSTRACT

The current approach for accurate determination for rare earth elements using environmental reference materials for k_0-INAA with short turnaround analysis times was investigated. The k_0 and Q_0 values for REEs, nuclear interference, and spectral interference were practically assessed and improved with the standard reference material. The evaluation of the current iterative neutron self-shielding and gamma-ray self-attenuation was established using reference material prepared from 100 mg/kg of 99.9% certified reference material (i.e., Alfa Aesar mono rare earth oxide combined with SiO_2). The general achievement of the current k_0-INAA technique for rare earth elements was validated with IAEA Soil-7 reference material and real sediment samples. The rare earth elements levels in the reference material range from 0.72 ± 0.08 mg/kg for ^{166}Ho to 60.8 ± 2.1 mg/kg for ^{141}Ce. The uncertainty at which the rare earth element concentration was examined is below 8% (at 95% confidence level). This showed good uniformity with the IAEA Soil-7 certified contents. In addition, k_0-NAA is able to quantify most of the REEs in real samples collected from three locations in Ghana.

1. INTRODUCTION

The instrumental neutron activation analysis (INAA) approach has been a widely used technique frequently employed for elemental analysis because of its numerous advantages [1, 3, 4]. The National Nuclear Research Institute (NNRI) of the Ghana Atomic Energy Commission (GAEC) has embraced this method as a standard analytical technique for assessing metalloids and radioactive elements in different environmental samples. The INAA at GAEC utilizes the 30 kW Ghana Research Reactor-1 (GHARR-1) built-in 1994, which generates neutron spectrum (i.e., thermal, epithermal, and fast neutrons). However, it has undergone core conversion in its present state. Thus, Ghana Research Reactor-1 operates at a half-power of 15 kW with 5.0 $\times 10^{11}$ cm^2.s as a corresponding thermal neutron flux [2]. The technique relies on high thermal neutrons flux and large cross-sections for (n,γ) reactions to provide good analytical sensitivity [1, 5]. Over the few decades, numerous laboratories worldwide have applied the k_0-standardization method of INAA (k_0-INAA) to suit the comparative procedures for quantifying analytes, which is considered the conventional quantitation method for INAA [7]. K_0-INAA is a single-comparator standardization method, which uses ^{197}Au, for precise analysis of elements in any sample matrix, without the requirement for recalibrating for all metalloids when analyzing new sample materials or employing new detectors [6].

A limited number of rare earth elements (REE's) including lutetium (Lu), ytterbium (Yb), terbium (Tb), europium (Eu), samarium (Sm), neodymium (Nd), cerium (Ce), and lanthanum (La) [8, 9] has been assessed using k_0-INAA, with research showing that k_0-

Corresponding author: aquisman1989@gmail.com

DOI: 10.21608/ajnsa.2021.91014.1504

INAA has the capability of computing exactly most of the REE's at the trace, minor and major concentrations [6]. REEs have numerous applications in many technologies, including electronic devices, permanent magnets, catalysts production, and other applications in the glass industry [6, 10, 11]. Therefore, knowledge about the presence and quantity of REEs in samples has become an economic advantage for industries exploring REEs. However, measuring REEs is demanding because of their similar properties (physical and chemical features) and low quantities [12]. Hence, one or two instrumental techniques, for instance, AAS, ICP-MS, ICP-OES, and NAA are used to assess REEs for precise identification and quantification [6, 13, 14]. For the past 25 years, the NNRI laboratory at GAEC has been exploring the use of k_0-INAA moderately. Due to the extensive cooling times required for REE to minimize spectral interferences, the conventional k_0-INAA technique has not been fully utilized to its capacity. Meanwhile, NNRI as a business-oriented research institution needs a highly accurate, precise, speedy assessment of samples and take advantage of Ghana's abundant mineral resources to explore REEs. Therefore, this research aims to validate the k_0-INAA performance to rare earth elements determination using two certified reference materials (i.e., Alfa Aesar mono rare earth oxide and IAEA Soil-7) and on real samples collected from three locations in Ghana.

2. METHOD OF CALCULATION AND THEORY

2.1 k_0-method of standardization

The k_0-NAA located at NNRI, GAEC uses the modified Hogdahl convention with the equation:

$$C(mg/kg) = \frac{peak\ area/t_c}{W\Phi_{th,eq}SDCBG_{eff}C_{mo}C_{temp}C_{\%full}C_{specInterf}C_{nuclInterf}} \quad \textbf{(1)}$$

Where W is the mass of the sample, $\Phi_{th,eq}$ is the thermal neutron flux equivalent to the thermal neutron flux observed by a Au monitor in the same irradiation channel, S is the saturation factor ($1\text{-}e^{-\lambda t_i}$), D is the decay factor ($e^{-\lambda t_d}$), C is the counting factor ($1\text{-}e^{-\lambda t_c}$)/$\lambda t_c$ where t_i, t_d, *and* t_c represent irradiation time, decay time and counting time, respectively. G_{eff} is the effective neutron self-shielding factor [19], B is the sensitivity factor, C_x represents correction factors used for sample neutron moderating effect, neutron temperature effect on reaction time, % sample filling factor, spectral and nuclear interferences. Most (n, γ) reactions possessed v^{-1} cross-section characteristics, and therefore the sensitivity factor of individual radioisotope, B, can be explained by equation 2. The sensitivity factor comprises k_0 and Q_0 values for the analyte, the ratio of the thermal and epithermal fluxes f, the epithermal neutron flux shape α, and the peak relative detection efficiency ε. Besides, the sensitivity factor relies on Avogadro's constant (N_{Av}) multiplied with the isotopic abundance of Au, gold radiative cross-section at 2200 m/s, γ-ray intensity of Au (411.8 keV), and the atomic mass of Au.

$$B = \frac{N_{AV}\theta_{AU}\sigma_{O,AU}I_{AU}}{M_{Au}} k_o \left(1 + \frac{Q_O(\alpha)}{f}\right)\varepsilon \quad \textbf{(2)}$$

Out of the non –1/v nuclides, ^{152}Eu, ^{152m}Eu, ^{169}Yb, and ^{177}Lu showed the farthest digression, and for that matter, these are analyzed with the k_0-NAA. The extended Hoghdal convention, which initiates newly computed values of Q_0, serves as the basis for the reactor moderator type and neutron temperature [6, 20]. The values of these are employed in co-occurrence with the nuclide-specific Westcott factor [$g(T_n)$] [6, 14]. To assess the k_0-NAA relevancy to REEs quantification in weight greater than 1g/kg, rare earth element concentrated samples, uncertainty, and many sources of systematic error were examined. These include Ghana Research Reactor-1 software, spectral interferences, neutron temperature effects, nuclear interferences for REEs, neutron self-shielding correction, and γ-ray self-attenuation correction. The software libraries of GHARR-1 activation analysis are designed based on the k_0-NAA technique and G_{eff} (i.e., Gunninck detection efficiency) model [6, 21]. The detection efficiency in the sensitivity factors (B) is implanted together with k_0 and Q_0 in the GHARR-1 software libraries.

2.2 Theory

2.2.1 Nuclear Interferences (NI)

The NI of REEs is produced predominantly from uranium-235 fission which yields light REEs. It is essential to be corrected because these interferences serve as a source of vital errors for uranium samples with content levels higher than 25 mg/kg, especially for metals with radionuclides that are products of fission reaction as lanthanum-140, cerium-141, cerium-143, and neodymium-147, respectively [6, 20]. That is to say it depends on the U/REE ratio. In this study, the correction factors were examined using a guaranteed standard uranium solution on filter paper. The results obtained from the computed uranium fission interference correction factors were compared with the literature values [15 – 17].

2.2.2 Gamma-ray self-attenuation effect

Gamma-ray self-attenuation can be explained as γ-ray emitted within the sample that is absorbed or scattered when the sample crosses on its way to the detector [20]. The γ-ray self-attenuation effect initiates errors, specifically gamma-rays with low energy in samples abundant in heavy metals. The gamma-ray self-attenuation effect for cerium-141, neodymium-147, samarium-153, dysprosium-165, and holmium-166 with gamma-ray energies less than 150 keV could be as high as 30%, and this was corrected using the Chilian et al. approach [19].

2.2.3 Thermal and Epithermal neutron self-shielding effect

High neutron absorptions cross-sections metalloids reduce the flux by the neutron self-shielding effect in the process of irradiation, for instance, samarium, europium, and gadolinium which are strong absorbers of thermal neutrons or isotopes like samarium-152, gadolinium-158, terbium-159, holmium-165, and thulium-169 with high resonances in the epithermal region [17]. An improved self-shielding iterative technique by Chilian et al. [19] was used to correct the thermal and epithermal self-shielding effect [6, 22, 23].

3. METHODOLOGY

The inner irradiation channels in the GHAR-1 facility mean thermal neutron flux, (Φ_{th}), enlarge from $(1.1404 \pm 0.051) \times 10^{11}$ to $(1.1831 \pm 0.063) \times 10^{11}$ $cm^2.s$. It was further re-quantify with copper wire monitors (10.0 mm long) with an estimated mass of 0.25 g each. It was observed that the thermal to epithermal neutron flux ratio (f) = 17.3 ± 0.5, while α, which stands for epithermal neutron flux shape factor = 0.033. Cadmium-ratio quantifications with 1.0 cm long IRMM Al-0.1% monitors with an estimated weight of 0.22 g each were used to validate f. The irradiation duration of the monitors was 10 min, and after 24 h decay time, counting was done 15 cm away from the detector surface.

To evaluate REEs concentrations in sample matrices, the standard solution was prepared from 100 mg/kg (certified Alfa Aesar Specpure), and 100 µL was pipetted on a Whatman 42 filter paper with dimensions of 1.2 cm by 10 cm using a plastic sheet as support. Time was taken between the starting of pipetting and weighing using a stopwatch [6]. A correction was conducted to check evaporation. The filter papers with the prepared standards were rolled into 0.8 cm diameter cylinders after drying. The rolled filter papers were placed into 1.5 cm long polyethylene vials and heat sealed. The prepared standard samples were transported to the reactor using a pneumatic transfer system operated at a pressure of 0.25 atm. The times for irradiation ranged from 25 sec to 7 h. The prepared standards were counted for 15 min, 1 h, 3 h, and 10 to 24 hr after cooling times of 30 min, 2 – 4 days, and 1 – 3 weeks after irradiation. The counting was achieved by using a PC-based gamma-ray spectrometry system that consists of 486 microcomputers for data assessment and analysis, emulation software card, and ACCUSPEC multichannel analyzer (MCA), and HPGe n-type coaxial detector. The operating bias voltage of the detector is (-ve) 3000 V with a relative efficiency of 25% and a resolution of 1.8 keV for ^{60}Co gamma-ray energy of 1332 keV. Spectral intensities of the prepared standards were collected and analyzed qualitatively to identify the radionuclides present, which was achieved using a multichannel analyzer card. Using gamma-spectrum analysis software SPAN 5.0, the area under the photopeak of each identified element was changed into concentration via calculation. The samples were counted for a longer duration to a total peak area with less than 0.2% systematic error.

To successfully complete the libraries (software information) for the spectral and nuclear interferences, the preparations of U and Th were carried out by the same procedure as the certified references material (certified Alfa Aesar Specpure). Neutron self-shielding and gamma-ray attenuation correction modules were confirmed using 0.1 g of pure rare earth oxides (99.9%), and it was followed by dilution with 2.0 g of silicon dioxide (SiO_2). Si and O are weak neutron moderators and neutron absorbers [6]. The default GHARR-1 activation analysis γ-ray detection efficiency model is already designed for SiO_2 matrix and ^{29}Al, with a half-life of 6.52 min, formed by $^{29}Si(n, p)^{29}Al$ and because of that, there is no interference during the analysis of REE. The samples of REE oxide were also irradiated in a neutron flux of 5.0×10^{11} $cm^{-2}s^{-1}$ for 25 s to 6 min. To prevent systematic errors initiated by coincidence summing, the oxides were calculated at a station labeled PA_3.

To check for the performance of the established method, 100 – 200 mg of IAEA Soil-7 reference material and real sediment samples collected from three different locations in Ghana were quantified. Six replicates of IAEA Soil-7 standards were prepared and packed together in a polyethylene rabbit capsule and heat sealed.

Each standard prepared from IAEA Soil-7 was placed in a separate capsule for short irradiation to capture elements like dysprosium and was assembled in one capsule for long-time irradiation. The method for preparing sediment samples for analyzing REEs was adapted by Dampare et al. [2]. At the laboratory, the dried sediment samples were grounded into a powdery form using mortar and pestle. Unwanted materials and large stones were discarded to lessen contamination. 50 mg of sediment sample were weighed into polyethylene foil, diluted with 2.0 g SiO_2, tied, and heated-sealed. The samples were loaded into a 7 mL-sized polyethylene rabbit capsule and heat-sealed. Each of the samples was placed in a separate capsule because they were irradiated for a short time. Each capsule was in succession packed in a 27 mL capsule sealed. The samples were then rounded off and heat-sealed. In each sample, 4 replicates were prepared. The process of irradiation, counting, and estimating the concentration followed the same procedure as the mono rare earth standard.

3.1 Effect of neutron temperature on the interaction rate with non-1/v nuclides

Even though most REEs are non-1/v thermal neutron absorbers, usually k_0-NAA can be used with high accuracy because thermal neutron (n,γ) cross-sections vary nearly as 1/v with changing reactor temperature. In contrast, the thermal neutron density obeys a Maxwell-Boltzmann distribution. The cross-section of the reactions $^{176}Lu(n,\gamma)^{177}Lu$, $^{151}Eu(n,\gamma)^{152}Eu$ and $^{168}Yb(n,\gamma)^{169}Yb$ possess a strong non-1/v characteristic, and the Westcott formalism for non-1/v nuclides is usually used by adding more complexity to the available method. Not long ago, the extended Høgdahl convention was suggested for including 1/v and non-1/v nuclides in a common method [6, 31]; it was embraced in the current study. Concerning non-1/v nuclides, the comparison of k_0 and Q_0 values employed in the GHARR-1 activation analysis libraries with the official k_0-NAA database [32] is outlined. The v represents the neutron velocity corresponding to a temperature Tn. Thus, in the following sections, "neutron temperature" is the average velocity of the thermal neutron density distribution corresponding to the temperature in the irradiation site [6]. Regarding non-1/v nuclides, the results were corrected from the default 30 °C to the true neutron temperature in the irradiation channel by applying the g(Tn) values in a Table compiled by van Sluijs et al. [31]. The neutron temperature was evaluated based on the reading of the reactor water outlet thermocouple. In this study, the neutron temperature varied from 26 °C to 55 °C. The errors in concentration presented by the uncertainty in the temperature ascertainment are calculated as 2.3% for ^{152}Eu, 1.5% for ^{169}Yb, and < 2% for ^{177}Lu.

4. RESULTS AND DISCUSSION

4.1 GHARR-1 activation analysis libraries and Sensitivity factors

The individual chemical element combined with the formed isotope, energy of the characteristic gamma-ray, and its half-life, GHARR-1 activation analysis libraries have three sensitivity factors, computed for a sample with a fixed geometry placed in three kinds of reproducible counting positions labeled, PA_1, PA_2, and PA_3. Table 1 shows the selection nuclides; isotopes formed, their gamma-rays, values of k_0, and Q_0 plus their uncertainty with a standard deviation of 1%. The data was fetched from the k_0 official database as cited in Whitty-Leveille et al. [24]. At the same time, the Q_0 values for europium-152, europium-152m, ytterbium-169, and lutetium-177 [20] and k_0 and Q_0 for thulium-170 was adapted from Abdollahi Neisiani et al. and Zawisza et al. [6, 25].

The GHARR-1activation analysis libraries look attentively at γ-ray self-attenuation correction for a sample density of 1000 mg/m^3, which is not the same as the real filter sample of 15 mg/m^3. Thus, to take into account this dissimilarity, new detection efficiencies were computed. The correction of neutron self-shielding is below 0.3% in all REEs; therefore, it wasn't corrected. The correction for actual-coincidence summing is necessary when k_0-NAA is used with low flux reactors resulting in close-counting geometries. The detection efficiency calibration and its true coincidence summing (COI) correction can be elaborated when assessing the data derived in position PA_1 because the performance model depends on the sample-detector geometry. The COI decreases below 2% as the interval between the sample and the detector increases. The results for individual REEs were normalized to the weighted content, and it was found that the range of each REE dataset was about 10%. The calculated value is the mean in this condition, with an uncertainty of 2% except for lutetium with 5% and europium 4%. Table 2 shows the average values of coincidence summing correction factors for all the counting positions PA_1, PA_2, and PA_3.

Table (1): Nuclear characteristics of rare earth element radioisotopes employed in this study [i.e., gamma energies, values of k_0, and Q_0 for target and formed isotopes] [19].

Target Isotopes	Formed Isotopes	half-life	γ-ray energy(keV)	k_0	(%; 1sd)	Q_0	(%; 1sd)
^{139}La	^{140}La	1.6781 d	1596.20	1.34E-01	1.10	1.24	5.00
^{140}Ce	^{141}Ce	32.508 d	145.40	3.66E-03	0.90	0.83	5.00
^{142}Ce	^{143}Ce	33.039 d	293.30	6.89E-04	0.50	1.20	5.00
^{141}Pr	^{142}Pr	19.120 h	1576.60	6.12E-03	0.60	1.51	5.00
^{146}Nd	^{147}Nd	10.980 d	91.10	1.02E-03	2.50	2.00	1.20
^{148}Nd	^{149}Nd	1.728 h	531.00	4.56E-04	1.10	2.00	1.20
^{152}Sm	^{153}Sm	46.284 h	103.20	2.31E-01	0.40	14.40	2.10
^{151}Eu	^{152}Eu	13.537 y	1408.00	9.36E+00	0.60	0.66	5.00
^{151}Eu	^{151m}Eu	9.3116 h	841.60	3.02E+00	5.00	0.66	5.00
^{152}Gd	^{153}Gd	240.40 d	103.20	4.54E-03	4.00	0.77	15.00
^{158}Gd	^{159}Gd	18.479 h	366.50	8.49E-04	1.60	29.90	3.10
^{159}Tb	^{160}Tb	72.30 d	879.40	8.25E-02	1.20	17.90	3.80
^{164}Dy	^{165}Dy	2.334 h	94.70	3.57E-01	0.90	0.19	3.80
^{165}Ho	^{166}Ho	26.830 h	80.60	4.94E-02	1.40	10.90	5.00
^{170}Er	^{171}Er	7.516 h	308.30	1.04E-02	2.50	4.42	2.40
^{169}Tm	^{170}Tm	128.60 d	84.30	3.45E-02[a]	5.00	14.3	3.30
^{168}Yb	^{169}Yb	32.026 d	198.00	1.04E-02	5.00	4.97	2.10
^{174}Yb	^{175}Yb	4.185 d	396.30	1.64E-02	0.60	0.46	5.00
^{176}Lu	^{177}Lu	6.648 d	208.40	7.14E-02	5.00	3.49	5.00

[a] k_0 and Q_0 values for ^{169}Tm, [16].

Table (2): Normalization of concentration for REE solutions on filter paper (Conc.$_{PA}$) relative to certified values (Conc.$_{cert}$) and their associated COI correction factors for counting positions PA_1, PA_2, and PA_3.

Formed Isotopes	γ-ray energy (keV)	Conc.$_{PA1}$/ Conc.$_{cert}$	COI$_{PA1}$	Conc.$_{PA2}$ / Con.$_{cert}$	COI$_{PA2}$	Conc.$_{PA3}$/ Conc.$_{cert}$	COI$_{PA3}$
^{140}La	1596.20	0.93	0.84	0.94	0.88	0.94	0.99
^{141}Ce	145.40	0.98	0.99	0.99	0.96	0.98	0.99
^{143}Ce	293.30	0.96	0.97	0.99	1.00	0.96	0.98
^{142}Pr	1576.60	0.97	0.99	1.03	0.97	1.05	0.99
^{147}Nd	91.10	1.00	0.97	0.99	0.99	1.01	0.99
^{147}Nd	531.00	0.99	0.99	0.99	0.97	0.99	0.98
^{153}Sm	103.20	0.96	0.98	1.00	0.99	0.97	1.00
^{152}Eu	1408.00	0.98	0.93	1.02	1.00	0.94	0.98
^{152m}Eu	841.60	0.99	0.91	1.02	0.97	0.98	1.00
^{153}Gd	103.10	1.00	1.00	0.99	0.99	1.00	0.99
^{159}Gd	366.50	0.96	0.99	0.98	0.98	1.00	0.99
^{160}Tb	879.40	0.99	1.00	1.03	0.97	1.01	1.00
^{165}Dy	94.70	0.98	1.02	0.99	0.99	0.98	0.99
^{166}Ho	80.60	1.01	0.99	1.01	0.98	1.00	0.98
^{171}Er	308.30	1.00	0.99	1.01	0.99	1.00	1.00
^{170}Tm	84.30	0.95	0.97	0.98	0.99	0.98	0.98
^{169}Yb	198.00	0.99	0.92	0.98	0.89	0.99	0.99
^{175}Yb	396.30	0.94	0.99	0.97	0.99	1.00	0.97
^{177}Lu	208.40	1.02	0.99	1.01	0.99	1.02	1.00

Considering the situation of free true COI isotopes: ^{141}Ce, ^{147}Nd (91.10 keV), ^{153}Sm, ^{165}Dy, ^{166}Ho, ^{170}Tm, and ^{153}Gd with energies less than 150 keV and those with relatively high energy γ-lines such as ^{142}Pr, ^{147}Nd (531.00 keV), ^{159}Gd, ^{169}Yb, and ^{175}Yb, the results from the analysis for station PA_1 and PA_3 exhibit total biases of 1 – 4% with uncertainty at 2 %. The detection efficiency model, as well as k_0 and Q_0 values, was validated using the results. Besides, the intensity factors of these REEs are precise for low and high-energy gamma-rays, including samples counted in far or close to detection geometry. Contrary, consistent negative biases of 3 – 5.5% were reported for the same formed isotopes results obtained for station labeled PA_2. Further experimental results were computed after the correction of the error for PA_2.

Also, the peaks of ^{177}Lu, ^{169}Yb, ^{171}Er, ^{160}Tb, ^{153}Gd, ^{152}Eu, ^{152m}Eu (841.60 keV), ^{143}Ce, and ^{140}La were based on summing-out true coincidence effects, whereas ^{152m}Eu (841.60 keV) and ^{175}Yb (396.30 keV) peaks were subjected to summing-in coincidence effect. ^{140}La and ^{171}Er show 3.5% negative biases, and this was observed in all results. This can be attributed to the imprecision of COI. These systematic errors were included in the uncertainty value because the bias in station labeled PA_1 will increase and direct to the COI as the origin of the error if the negative bias in station marked PA_3 for ^{143}Ce is accounted for by limiting the sensitivity factor.

Since biases in station PA_3 were less than 1%, coincidence summing correction factors over-corrects for 152-Eu (1408.00 keV) and 160-Tb (879.40 keV) were counted in station PA_1. The uncertainty of this event was included in the uncertainty estimate of results obtained through the terbium-160 (879.40 keV) gamma-line. According to Ravisanker et al. [26], with the expectation that values of Q_0 and $g(T_n)$ are within the acceptable range, the results for the 152-Eu (1408.00 keV) certify that its k_0 score is adequately correct. Unlike 152m-Eu (841.60 keV), the factor of k_0 was located around 2.79; the value is 9.6% greater than one found in the official database as cited in Whitty-Leveille et al. [24]. When assessing the efficiency of the sensitivity factors and the detection model, the values of k_0 and Q_0 of ^{177}Lu (208.40 keV) the experimental value obtained in positions labeled PA_1 and PA_3 gave a bias within the 6.2% limit of computed uncertainty. GHARR-1 activation analysis software does not consider the conditions when the values of k_0 were computed differently; for instance, the nuclides related with decay type IV/b corresponding to "two-component decay" which move in a metastable state is significantly lower half-life than that of the ground state used in the assessment process. Furthermore, GHARR-1 activation analysis deals with all reactions as "beta-beta" or type I except few situations where an established correction factor is used for a default decay time (^{80}Br, ^{99}Mo, and ^{115}Cd).

4.2 Correction factors for C_{mo} and $C_{\%}$

C_{mo} and $C_{\%}$ were ignored in this work because the correction factor for the sample neutron moderating effect (C_{mo}) was unity. The reason is that moderator materials (e.g., H) are absent in the samples. Also, there is no thermalization of epithermal and fast neutrons, which collides with the moderating atoms resulting in a change of the neutron flux. However, the % sample filling factor ($C_{\%}$) was unity because the 100% filling factor of the vial was used to prepare all samples. Thus, the counting geometry could be reproduced, and the systematic inaccuracy initiated by the detection efficiency model for lower filling factors was prevented [6, 24, 26].

4.3 Correction factor for neutron temperature

The activation rate difference due to a change of neutron radiative capture cross-section with neutron temperature is called the C_{temp} [6]. The neutron flux detector in GHARR-1 activation analysis is self-powered by cadmium. As the ^{235}U fission rate with thermal neutrons and reflector moderating characteristics decreased with an increased reactor temperature, the reactor's control rod draws out for keeping a uniform electrical current from the cadmium neutron detector is equal to the thermal activation rate constant. It was found that there has been a change in the shape of the neutron spectrum and the rate of thermal to epithermal neutron flux, f which was produced in both actions, including an increase of temperature and withdrawal of the control rod. Considering *1/v* nuclides, the C_{temp} was carried out based on a reading of the reactor water outlet and inlet thermocouples, and it varied from 0.8% - 3.5%. Because epithermal neutron flux and α decreased with increased temperature, the correction initiates a small systematic error (< 2 %) for nuclides with values of Q_0 greater than 30.

4.4 Correction factor for spectral interference

To add to sensitivity factors, GHARR-1 activation analysis old libraries contained few corrections for spectral as exhibited in Table 3 (correction factors for spectral interference for 3 different counting stations labeled PA_1, PA_2, and PA_3 for the data distinct with superscript "z"). For instance, ^{141}Ce (145.40 keV) γ-line interfered with by ^{175}Yb (396.30 keV) γ-line, and the correction factor was initiated immediately after the counting at station PA_1. The decay of neptunium-239 is used to compute uranium with a gamma-ray at 106.2 keV, which interfered with samarium-153 (103.2 keV), and a correction was provided during the counting at a station marked PA_2. The various correction factors were significant for all counting stations, precisely samples of high REE content, which impose counting beyond the detector at station PA_3. The experimental assessment becomes convenient when there are accurate correction factors because it removes the errors initiated by the detection and counting geometry models and true-coincidence summing. When the experimental technique is inconvenient, the correction factors were computed from the γ-ray wavelengths and their associated detection efficiency. The fission product of uranium-235, which was the isotope ^{133}I, interfered with neodymium-147 (531.00 keV) in uranium-bearing matrices. This condition was overlooked for samples with high neodymium content depleted in uranium, and some cases were prevented by increasing the decay time, for instance, the interference of ^{153}Sm with ^{147}Nd 91.10 keV. The isotope ^{131}I, the fission product of ^{235}U, depicted a significant spectral interference for ^{159}Gd (366.50 keV) peak. There were interference cases of ^{233}Pa on the 94.70 keV of ^{165}Dy. When the statistical uncertainty of the surface of the inferring peak is higher than 20%, correction factors are calculated for individual counting stations and included in the library. Table 3 shows the current spectral interference correction factors which were practically computed.

Table (3): Correction factors for spectral interference recorded in the various counting stations (PA_1, PA_2, and PA3).

Formed Isotope	γ-ray energy (keV)	half-life	Spectral interference Isotope	γ-ray energy$_{SIIinterf}$ (keV)	γ-ray energy$_{SII}$ (keV)	Decay time	PA_1	PA_2	PA_3
^{141}Ce	145.40	32.51 d	^{175}Yb	321.60	282.70	3.48 d	0.051	0.094	0.086
^{147}Nd	91.10	10.98 d	^{153}Sm	497.80	341.10	69.5 h	0.013	0.009	0.014
			^{133}I (U)	562.60	901.90	15.9 h	27.5	23.1	25.2
^{153}Sm	103.20	46.28 h	^{233}Pa	124.00	492.10	22.5 d	0.071^{z}	0.069	0.069
			^{239}Np(U)	99.40	199.50	7.87 d	0.995^{z}	1.084	1.092
^{159}Gd	363.50	18.45 h	^{131}I ($U_{fission}$)	401.20	708.80	14.2 d	9.56	9.72	10.11
^{160}Tb	796.20	72.30 d	^{233}Pa (Th)	299.40	297.10	19.3 d	0.346	0.342	0.341
^{165}Dy	99.40	2.334 h	^{233}Pa	109.30	384.70	9.44 d	0.111	0.132^{z}	0.126

^{z} Actual correction factors for spectral interference in the old GHARR-1 activation analysis library

4.5 Correction factor for nuclear interference

Because there was a reasonable concentrated amount of rare earth elements in the samples and irradiated for just a few minutes in a low neutron flux reactor [27], the nuclear interferences from the second-order reactions were insignificant. [6, 28] both opined that samples accommodating uranium, rare earth elements, for instance, lanthanum, cerium, and neodymium, can be influenced by interferences due to fission if the uranium level is more than those of light rare earth elements. In this circumstance, isotopes such as ^{140}La, ^{141}Ce, and ^{147}Nd that were selected for computing the concentration of the associated elements were also obtained from the fission process of uranium. The correction factors for nuclear interference were evaluated by calculating the quantity of individual isotope produced divided by a unit mass of standard uranium. Table 4 explains the REEs influenced by interferences from uranium fission. Abdollahi Neisiani et al. [6] and Tiwari et al. [8] recently proposed the calculated theoretical values measured from REE fission and the correction factors for uranium interference calculated in this study.

4.6 Neutron self-shielding and Gamma-ray self-attenuation

REE oxides are employed to examine the correction models for γ-ray self-attenuation and neutron self-shielding in extreme situations. To prevent systematic errors initiated by the detection efficiency model for a close-counting geometry, the REE oxides samples were recorded 10 cm off the detector at the counting station labeled PA_3. GHARR-1 activation analysis libraries presume a silicon dioxide matrix of density equivalent to 1.00 kg/m^3. Gamma-ray self-attenuation is quantified using the true density of the sample and its composition to avoid biases as much as 26% for elements evaluated with nuclides releasing low-energy gamma-rays. An iterative technique was executed in this current work to correct γ-ray self-attenuation for samples which composition is unknown. To make the calculation more straightforward, it is presumed that the mean path of gamma-ray in the sample is equivalent to one-half of the mean sample thickness. The attenuation coefficient comprises material density, sample constituent, and gamma-ray energy. The matrix mass attenuation coefficient for individual gamma-ray energy was calculated using elemental mass attenuation coefficients adapted from the national institute of standards and technology tables [29] and the Beer-Lambert law. Table 5 shows the results of the γ-ray self-attenuation technique for the high content mono-rare earth element.

Table (4): Uranium fission interference correction factors for rare earth elements

Element	Formed Isotope	γ-ray energy (keV)	Theoretical	Tiwari et al. [8]	Abdollahi Neisiani et al. [6]	GHARR-1	This study
La	^{140}La	1596.20	0.016	0.0027	0.00231	0.00246	0.00218
Ce	^{141}Ce	145.40	0.280	0.34	0.282	0.279	0.284
	^{143}Ce	293.30	1.330	1.35	1.28	1.291	1.276
Nd	^{147}Nd	91.100	0.220	0.20	0.190	0.199	0.191

Table (5): Comparisons of quantified rare earth element concentrations in SiO_2 with certified values ($Conc._{cert}$) at the various sequence of k_0-NAA: content obtained from GHARR-1 ($Conc._{GHARR1}$), after correction for self-shielding ($Conc._{CSS}$), and after correction for γ-ray attenuation ($Conc._{CGA}$).

Formed Isotope	γ-energy (keV)	$Conc_{cert}$ (% wt)	$Conc_{GHARR1}$/ $Conc_{cert}$	$Conc._{CSS}$/ $Conc._{cert}$	$Conc._{CGA}$/ $Conc._{cert}$
^{140}La	1596.20	0.91	0.91	1.02	1.03
^{141}Ce	145.40	0.84	0.87	0.94	0.96
^{143}Ce	293.30	0.89	0.82	0.88	0.91
^{142}Pr	1576.60	0.91	0.49	0.81	0.90
^{147}Nd	91.10	0.81	0.92	0.93	0.98
^{147}Nd	531.00	0.85	0.87	0.91	0.94
^{153}Sm	103.20	0.87	0.65	0.81	0.92
^{152}Eu	1408.00	0.89	0.82	0.83	0.92
^{152m}Eu	841.60	0.90	0.69	0.79	0.91
^{159}Gd	103.20	0.86	0.77	0.98	0.99
^{159}Gd	366.50	0.88	0.57	0.86	0.91
^{160}Tb	879.40	0.84	0.83	0.89	0.97
^{165}Dy	94.70	0.90	0.82	1.02	1.02
^{166}Ho	80.60	0.86	0.66	0.91	0.99
^{171}Er	308.30	0.83	0.59	0.79	0.93
^{170}Tm	84.30	0.89	0.81	0.89	0.97
^{168}Yb	198.00	0.82	0.88	0.89	0.94
^{174}Yb	396.30	0.83	0.64	0.91	0.96
^{177}Lu	208.40	0.93	0.96	1.00	1.02

4.7 Validation of k_0-Neutron Activation Analysis for rare earth elements

The efficiency of the k_0-NAA for measuring REEs was examined with IAEA Soil-7 reference materials, and the results are outlined in Table 6. Acceptance of the element concentration obtained after the analysis by k_0-NAA with the IAEA Soil-7 certified values was tested with the E_n numbers by International Standard Organisation Guide 13538 [30]. E_n score performance testing evaluates a participant's ability to have laboratory values close to certified values within their claimed expanded uncertainty. This performance statistic is calculated as:

$$(En) = \frac{Xi - Xpt}{\sqrt{\{U^2(Xi) + U^2(Xpt)\}}} \quad \textbf{(3)}$$

Where X_i represents the laboratory value, X_{pt} is the certified value, $U(X_i)$ uncertainty of the laboratory value, and $U(X_{pt})$ uncertainty of the certified value. If E_n scores $\geq$ 1.0 or $E_n \leq$ -1.0, indicate a need to review the uncertainty estimates or correct a measurement issue, and if $-1.0 < E_n < 1.0$ shows successful performance.

Table (6): Comparisons of quantified rare earth elements concentrations (Conc.$_{lab}$) with certified values (Conc.$_{cert}$) at various sequence of k_0-NAA: content obtained from GHARR-1 (Conc.$_{GHARR1}$), after correction for self-shielding (Conc.$_{CSS}$) and after correction for γ-ray attenuation (Conc.$_{CGA}$).

Element	Formed Isotope	γ-ray energy (keV)	Conc.$_{cert}$ ±Δ(mg/kg)	Conc.$_{GHARR1}$/ Conc.$_{cert}$	Conc.$_{CSS}$/ Conc.$_{cert}$	Conc.$_{CGA}$/ Conc.$_{cert}$	Conc.$_{lab}$ ±Δ(mg/kg)	E_n
La	^{140}La	1596.20	28.5 ± 1.1	0.94	0.97	0.98	27.8 ± 1.2	-0.43
Ce	^{141}Ce	145.40	60.8 ± 2.1	0.96	0.97	0.99	59.4 ± 2.6	-0.42
Ce	^{143}Ce	293.30	59.4 ± 2.4	0.92	0.96	0.99	58.7 ± 1.9	-0.23
Pr	^{142}Pr	1576.60	7.5 ± 0.6	0.94	0.95	0.97	7.44 ± 2.6	-0.02
Nd	^{147}Nd	91.10	27.2 ± 1.2	0.93	0.94	0.97	26.81 ±1.4	-0.21
Nd	^{147}Nd	531.00	26.7 ± 0.9	0.94	0.96	0.98	25.4 ± 0.5	-1.26
Sm	^{153}Sm	103.20	4.34 ± 0.4	0.91	0.94	0.96	4.15 ± 0.3	-0.76
Eu	^{152}Eu	1408.00	1.7 ± 0.3	0.94	0.98	0.99	1.63 ± 0.2	-0.19
Eu	^{152m}Eu	841.60	1.2 ± 0.05	0.96	0.98	1.00	1.2 ± 0.04	0
Gd	^{159}Gd	103.20	4.89 ±0.16	0.94	0.95	0.97	4.66 ±0.21	-0.87
Gd	^{159}Gd	366.50	4.21 ±0.56	0.99	1.01	1.02	4.04 ±0.37	-0.38
Tb	^{160}Tb	879.40	1.0 ± 0.02	0.97	0.98	0.98	0.98 ±0.03	-0.56
Dy	^{165}Dy	94.70	3.8 ± 0.18	0.99	1.00	1.01	3.82 ±0.15	0.09
Ho	^{166}Ho	80.60	0.72 ±0.08	0.94	0.96	0.98	0.69 ±0.13	-0.20
Er	^{171}Er	308.30	2.46 ±0.11	-	-	-	2.23 ±0.21	-0.97
Tm	^{170}Tm	84.30	0.54 ±0.03	1.00	1.00	1.01	0.56 ±0.03	0.48
Yb	^{175}Yb	396.3	2.60 ±0.12	0.89	0.94	0.96	2.47 ±0.13	-0.74
Lu	^{177}Lu	208.40	0.74 ±0.04	0.95	0.99	0.99	0.71 ±0.05	-0.47
Th	^{233}Pa	354.25	1.47 ±0.08	1.01	1.02	1.02	1.48 ±0.06	0.1
U	^{239}Np	399.82	0.88 ±0.03	-	-	-	0.82 ±0.05	-1.05

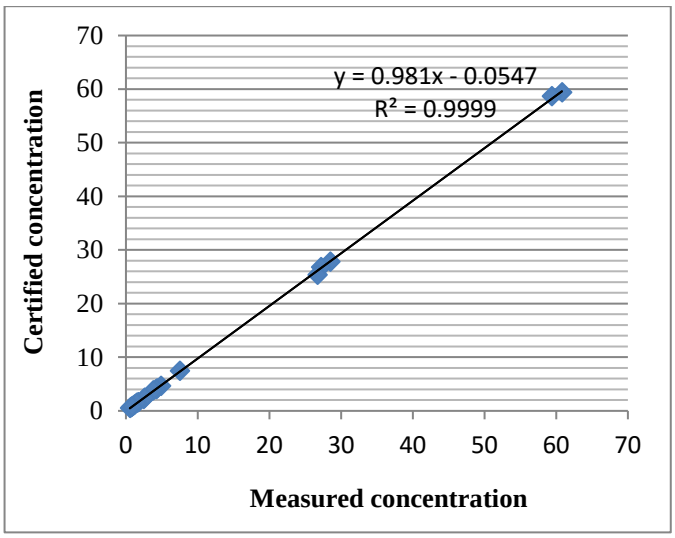

Fig. (1): The correlation coefficient for the linear regression between certified and measured concentrations.

Table 7 shows the general combination of standard uncertainty measured.

Table (7): Uncertainty compositions for the assessment of IAEA Soil-7 by k_0-NAA method

Source of Uncertainty	Representative range
Sample mass	0.20%
$k_0\,(g(T_n) + Q_0\,(\alpha)/f)$	1.0% - 6.5%
Counting statistics	0.15% - 25%
DE (geometry effects)	0.5% - 3.0%
DE (gamma-ray self-attenuation)	0.1% - 4.0%
ICD	0%
Interferences (Gamma-ray)	0.2%
Interferences (Fission)	0.3%
NTE	0.16% - 4.5%
NSS	0.36 – 2.5%

DE stands for Detection efficiency; ICD represents Irradiation, Counting and Decay time; NTE stands for neutron temperature effects; NSS stands for Neutron Self-Shielding.

Table (8): Average concentration of REEs (mg/kg d.w) detected in real sediment samples (n = 4)

REEs	Formed Isotope	γ-ray energy (keV)	Sample 1	Sample 2	Sample 3
La	^{140}La	1596.20	11.21 ± 0.41	6.51 ± 0.21	10.19 ± 1.01
Ce	^{141}Ce	145.40	9.10 ± 0.11	13.06 ± 1.22	n.d
Ce	^{143}Ce	293.30	13.2 ± 0.37	29.61 ± 3.02	n.d
Pr	^{142}Pr	1576.60	5.09 ± 0.44	18.04 ± 1.94	22.03 ± 2.81
Nd	^{147}Nd	91.10	10.01 ± 0.23	31.01 ± 2.75	8.19 ± 0.35
Nd	^{147}Nd	531.00	n.d	6.77 ± 0.49	13.52 ± 0.42
Sm	^{153}Sm	103.20	n.d	9.08 ± 0.52	9.06 ± 0.28
Eu	^{152}Eu	1408.00	3.71 ± 0.21	11.02 ± 0.37	5.75 ± 0.2
Eu	^{152m}Eu	841.60	n.d	n.d	2.11 ± 0.34
Gd	^{159}Gd	103.20	8.01 ± 0.16	8.25 ± 0.38	3.17 ± 0.11
Gd	^{159}Gd	366.50	16.69 ± 0.43	n.d	n.d
Tb	^{160}Tb	879.40	n.d	n.d	n.d
Dy	^{165}Dy	94.70	n.d	n.d	n.d
Ho	^{166}Ho	80.60	18.54 ± 0.94	12.02 ± 0.84	4.07 ± 0.35
Er	^{171}Er	308.30	9.85 ± 0.85	5.88 ± 0.42	9.03 ± 0.95
Tm	^{170}Tm	84.30	17.11 ± 0.41	9.73 ± 0.89	7.05 ± 0.28
Yb	^{175}Yb	396.3	20.07 ± 1.04	28.02 ± 2.03	13.07 ± 1.04
Lu	^{177}Lu	208.40	1.33 ± 0.12	6.01 ± 0.35	1.17 ± 0.04
Th	^{233}Pa	354.25	n.d	3.11 ± 0.13	1.44 ± 0.03
U	^{239}Np	399.82	0.97 ± 0.11	2.04 ± 0.28	1.02 ± 0.11

n.d denotes “not detected”

Based on the E_n values obtained, discrepant results were noticed for neodymium calculated with ^{147}Nd (237.51 keV) with E_n = -1.26 and neptunium measured with ^{239}Np (304.70 keV) with E_n = -1.05. The results obtained with ^{147}Nd (237.51 keV) and ^{239}Np (304.70 keV) corresponds to position with a label PA_1, and the true coincidence correction could be attributed for the slight variation of -1.26 for Nd and -1.05 for Np. The E_n results for other REEs were found within the acceptable performance. This means the laboratory values are in agreement with the certified values. The correlation coefficient for the linear regression between certified and measured concentrations = 0.999 (see Figure 1). The uncertainty at which the REE concentration was examined is below 8% (at 95% confidence level) (Table 7). Although most laboratory values were slightly smaller than the certified values, based on the *En* values and correlation coefficient for the linear regression between certified and measure values, it indicates an almost complete balance of the recovery standard. This shows a complete extraction, minimal losses, good alignment between spiking and calibration solution, and the analytical technique [33, 34]. Hence, k_0-INAA can quantify the REEs concentration in IAEA Soil-7. k_0-NAA passed to quantify most of the REEs in real samples collected from three locations (Table 8). The not detected REEs in each sample may be due to their concentration at mg/kg level, low energy gamma-lines, and short decay time.

5. CONCLUSION

The INAA method has been proven to be very reliable in the assessment of REEs in IAEA Soil-7. The study has also proved that the instrumental neutron activation analysis facility of the NNRI, GAEC is convenient for evaluating rare earth elements of Ghanaian environmental samples.

Acknowledgements

The authors would like to acknowledge the staff of Ghana Research Reactor-1 facility, National Nuclear Research Institute at Ghana Atomic Energy Commission (GAEC), and colleagues at the Department of Nuclear & Science Applications, Graduate School of Nuclear and Allied Sciences, the University of Ghana-Atomic campus for their non-financial support.

REFERENCES

[1] B.S. Wee, M. Ebihara, Neutron activation analysis and assessment of trace elements in fingernail from residents of Tokyo, Japan". Sains Malaysiana, 46(4):605-613; (2017). http://dx.doi.org/10.17576/jsm-2017-4604-13

[2] S.B. Dampare, D.K. Asiedu, S. Osae, B.J. Nyarko, B. Banoeng-Yakubo, Determination of rare earth elements by neutron activation analysis in altered ultramafic rocks from the Akwatia District of the Birim diamondiferous field, Ghana, Journal of Radioanalytical and Nuclear Chemistry,Vol. 265, No. 1,101–106; (2005)

[3] H.P. Chai, N. Lee, J. Grinang, T.Y. Ling, S.F. Sim, Assessment of heavy metals in water, fish, and sediments of the Baleh River, Sarawak, Malaysia. Borneo Journal of Resource Science and Technology, 8(1): 30-40; (2018). https://doi.org/10.33736/bjrst.822.2018

[4] B.S. Wee, S.A. Rahaman, M.S. Elias, et al., K_0-Instrumental Neutron Activation Analysis Method Validation for Trace Element Determination using Environmental Reference Materials, Borneo Journal of Resource Science and Technology, 9(2): 107-114; (2019).

[5] K. Gyamfi, B.J.B. Nyarko, S.A. Bamford, G. Owiredu, E. Ampomah-Amoako, Experimental evaluation of the variation of gamma-ray self-attenuation correction factor with gamma energy and geometry of analytical sample, Journal of Analytical Science & Technology, (2012). http://dx.doi.org/10.5355/JAST.2012.160

[6] M. Abdollahi Neisiani, M. Latifi, J. Chaouki, C. Chilian, Novel approach in k0-NAA for highly concentrated REE Samples, Talanta, 180:403 – 409; (2018).

[7] F. De Corte, The k0-standardization of NAA: germs, launch, breakthrough - on stage and in the wings. Journal of Radioanalytical and Nuclear Chemistry, 318(3): 1559-1563; (2018).

[8] S. Tiwari, A.G.C. Nair, R. Acharya, A.V.R. Reddy, A. Goswami, Analysis of uranium-bearing samples for rare earth and other elements byk0-based internal mono standard INAA method, Journal Nuclear and Radiochemistry Science, 8 (1):25–30; (2007).

[9] C. Xiao, Y. Yao, X. Jin, et al., k0-NAA for determination of REE in reference materials of ore sources, Journal of Radioanalytical and Nuclear Chemistry, 311 (2)1287–1289; (2017).

[10] European Commission, Report on Critical Raw Materials for the EU, Report of the Ad hoc Working Group on Defining Critical Raw Materials.

[11] D. Bauer, D. Diamond, J. Li, D. Sandalow, P. Telleen, B. Wanner. Department of Energy Critical Materials Strategy, United States, 2010.

[12] W.F. McDonough, S.-s. Sun, The composition of the Earth, Chem. Geol., 120 (3–4) 223–253; (1995).

[13] E.A Asare, Z B. Assim, R.B.Wahi, et al., Geochemistry examination of surface sediments from Sadong River, Sarawak, Malaysia: Validation of ICP-OES Assessment of Selected Heavy Metals, Eurasian Journal of Analytical Chemistry, 14(3): emEJAC-00337; (2019).

[14] J.A. D'Angelo, L.D. Martinez, S.E. Resnizky, E. Perino, E.J. Marchevsky, Determination of eight lanthanides in apatites by ICP-AES, XRF, and NAA, J. Trace Microprobe Tech., 19 (1) 79–90; (2001). online: 16 Feb 2007. https://doi.org/10.1081/TMA-100001463

[15] F.F. Arboccò, P. Vermaercke, K. Smits, L. Sneyers, K. Strijckmans, Experimental determination of k0, Q0 factors, effective resonance energies, and neutron cross-sections for 37 isotopes of interest in NAA. Journal of Radioanalytical and Nuclear Chemistry, 302(1): p. 655-672; (2014).

[16] J. St-Pierre, G. Kennedy, Re-measurement of Q_0 and k_0 values for 14 nuclides. Nuclear Instruments and Methods in Physics Research Section A: Accelerators, Spectrometers, Detectors, and Associated Equipment, 564(2): p. 669-674; (2006). https://doi.org/10.1016/j.nima.2006.04.019

[17] M. Abdollahi Neisiani, Quantifying rare earth elements content in high concentrated samples by k0-NAA, Department De Genie Chimique, Ecole Polytechnique De Montreal, Quebec, Canada, (2017).

[18] C. Westcott, Effective cross-section values for well-moderated thermal reactor spectra. (Corrected), Atomic Energy of Canada Ltd., Chalk River, Ontario (Canada), (1990).

[19] C. Chilian, J. St-Pierre, G. Kennedy, Complete thermal and epithermal neutron self-shielding corrections for NAA using a spreadsheet. Journal of radioanalytical and nuclear chemistry, 278(3): p. 745-749; (2008). doi: 10.1007/s10967-008-1604-8

[20] A. Santoro, V. Thoss, S. Ribeiro Guevara, Assessing rare earth elements in quartz-rich geological samples. Applied Radiation and Isotopes, 107: p. 323-329; (2016).

[21] E. Bulska, B. Danko, R.S. Dybczynski, et al., Inductively coupled plasma mass spectrometry in comparison with neutron activation and ion chromatography with UV/VIS detection for the determination of lanthanides in plant materials. Talanta, 97: p. 303-311; (2012).

[22] S. Kafala, T. MacMahon, Comparison of neutron activation analysis methods. Journal of radioanalytical and nuclear chemistry, 271(2): p. 507-516; (2007). https://doi.org/10.1007/s10967-007-0238-6

[23] R.S. Dybczyński, E. Czerska, B. Danko, K. Kulisa , Z. Samczyński, Comparison of performance of INAA, RNAA and ion chromatography for the determination of individual lanthanides, Appl. Radiat. Isot., 68 (1) 23–27; (2010).

[24] L. Whitty-Léveillé, K. Turgeon, C. Bazin et al., A comparative study of sample dissolution techniques and plasma-based instruments for the precise and accurate quantification of REEs in mineral matrices. Analytica Chimica Acta, 961: p. 33-41; (2017).

[25] B. Zawisza, K. Pytlakowska, B. Feist, M. Polowniak, A. Kita, R. Sitko, Determination of rare earth elements by spectroscopic techniques: a review. Journal of Analytical Atomic Spectrometry,; 26(12): p. 2373-2390; (2011). https://doi.org/10.1039/C1JA10140D

[26] R. Ravisankar, E. Manikandan, M. Dheenathayalu, et al., Determination and distribution of rare earth elements in beach rock samples using instrumental neutron activation analysis (INAA). Nuclear Instruments and Methods in Physics Research Section B: Beam Interactions with Materials and Atoms, 251(2): p. 496-500; (2006). https://doi.org/10.1016/j.nimb.2006.07.021

[27] H.G. Stosch, Neutron Activation Analysis of the Rare Earth Elements (REE) – With Emphasis on Geological Materials, in Physical Sciences Reviews, (2016). https://doi.org/10.1515/psr-2016-0062

[28] M.D. Glascock, P.I. Nabelek, D.D. Weinrich,et al., Correcting for uranium fission in instrumental neutron activation analysis of high-uranium rocks. Journal of Radioanalytical and Nuclear Chemistry, 99(1): p. 121-131; (1986).

[29] O. Shulyakova, P. Avtonomov, V. Kornienko, New developments of neutron activation analysis

applications. Procedia-Social and Behavioral Sciences, 195: p. 2717-2725; (2015). doi: 10.1016/j.sbspro.2015.06.380

[30] ISO Guide, 13528 Statistical methods for use in proficiency testing by interlaboratory comparisons, ISO, Geneva, (2005).

[31] R. van Sluijs, Q0's and resonance energies used in k0-NAA compared with estimations based on ENDF/B-VII.1 cross section data. Journal of Radioanalytical and Nuclear Chemistry, 309 (1):219–228; (2016).

[32] R. Jaćimović, F. De Corte, G. Kennedy, P. Vermaercke, Z. Revay, The 2012 recommended k0-database, Journal of Radioanalytical and Nuclear Chemistry, 300(2):589–592; (2014).

[33] E.A. Asare, R. Wahi, A.O. Gyampoh, O.A. Omorinoye, Determination of rare earth elements and its distribution pattern from the core sediments by k_0-instrumental neutron activation analysis. Indian Journal of Environmental Protection, 41(7):738–744; (2021).

[34] E.A. Asare, Impact of the illegal gold mining activities on Pra River of Ghana on the distribution of potentially toxic metals and naturally occurring radioactive elements in agricultural land soils. Chemistry Africa 1–18; (2021). https://doi.org/10.1007/s42250-021-00285-1